Earth and Planetary Science Letters 319-320 (2012) 251–258

Contents lists available at SciVerse ScienceDirect

Earth and Planetary Science Letters

journal homepage: www.elsevier.com/locate/epsl

Framboidal iron oxide: Chondrite-like material from the black mat, Murray Springs, Arizona

Mostafa Fayek [a,*], Lawrence M. Anovitz [b], Lawrence F. Allard [c], Sharon Hull [d]

[a] Department of Geological Sciences, University of Manitoba, 240 Wallace Building, Winnipeg, Canada MB R3T 2N2
[b] Chemical Sciences Division, ORNL, Oak Ridge, TN 37831-6110 USA
[c] Materials Science and Technology Division, ORNL, Oak Ridge, TN 37831 USA
[d] Department of Anthropology, University of Manitoba, Winnipeg, Canada MB R3T 2N2

ARTICLE INFO

Article history:
Received 26 January 2011
Received in revised form 16 November 2011
Accepted 22 November 2011
Available online 21 January 2012

Editor: L. Stixrude

Keywords:
Younger-Dryas
Clovis
meteorite
framboids
chondrite
black-mat

ABSTRACT

At the end of the Pleistocene a Younger Dryas "black mat" was deposited on top of the Pleistocene sediments in many parts of North America. A study of the magnetic fraction (~10,900 ± 50 B.P.) from the basal section of the black mat at Murray Springs, AZ revealed the presence of amorphous iron oxide framboids in a glassy iron-silica matrix. These framboids are very similar in appearance and chemistry to those reported from several types of carbonaceous chondrites. The glass contains iron, silicon, oxygen, vanadium and minor titanium, while the framboidal particles contain calcium as well. The major element chemistry of both the spherules and the glass matrix are consistent with the chemistry of material associated with meteorite impact sites and meteorites. Electron microscopy confirms that the glassy material is indeed amorphous, and also shows that what appear to be individual oxide particles are amorphous as well. The latter appears consistent with their overall morphology that, while euhedral, typically shows significant fracture. Based on these data, we argue that these particles are the product of a hypervelocity impact.

1. Introduction

Approximately 13,000 years ago the landscape of North America was very different from that which exists today (e.g., Alley, 2007; Haynes, 2008). The Clovis people, identified in the archeological record by large, unique projectile points recovered throughout North America, were hunting mammoths and other megafauna that roamed the continent near the close of the Pleistocene (Haynes, 2008). After 12,900 years ago, however, neither these large mammals nor the material remains of the Clovis inhabitants appear in the geological or archeological records. Instead Folsom-style artifacts appear to have replaced Clovis (Haynes, 2008; Meltzer and Holliday, 2010). This coincides with a period in which the Younger Dryas (YD) climate was significantly colder than either the preceding late-Pleistocene (Allerød) or the succeeding early-Holocene (pre-Boreal). First recognized in pollen profiles from northern Europe, this cold reversal was named the Younger Dryas after fossil pollen of the dryas plant (*Dryas octopetala*), signifying a tundra flora, commonly found in its fossil pollen assemblages (Taylor and Lamorey, 1993). Radiocarbon ages for the YD vary, but dates of approximately 10,900 ± 50 B.P. for its beginning and 9800 ± 50 B.P. (12,900 years ago) for its end are reasonable (Fiedel, 2006; Haynes, 2008; Stuiver et al., 1995). There have been several hypotheses presented to explain these sudden changes in climate and human culture, as well as the late-Pleistocene extinction, and some are highly controversial (e.g., Alley, 2000, 2007; Bradley and England, 2008; Broecker, 2006; Broecker et al., 1985, 1989; Firestone et al., 2007; Gill et al., 2009; Kennett et al., 2008, 2009; Marlon et al., 2009; McManus et al., 2004; Pinter and Ishman, 2008). Nevertheless, it is clear that a major paleoenvironmental event occurred at ~12,900 years ago.

One of the geological markers often associated with the YD onset is a dark, organic-rich layer of clayey silt called the "black mat" (Firestone et al., 2007; Haynes, 2008; West and Goodyear, 2008). Black mats are found in two-thirds of the 97 geoarcheological sites that bridge the Pleistocene–Holocene transition (Haynes, 2008). Most black mats are paleosols, but some consist of a layer of organic material, varying in color from dark gray to black, considered to have been deposited under moist to wet conditions. Clovis artifacts and Pleistocene fauna are found directly beneath, but never within or above, the black mat (Haynes, 2008). Most YD-age black mats are dark gray to black due to relatively high organic carbon (0.05–8%) compared with strata above and below (Essene and Fisher, 1986; Lougheed and Mancuso, 1973). There are both younger and older black layers (Holliday and Meltzer, 2010), but they do not appear to be as common, pervasive or as widely distributed over North America

* Corresponding author. Tel.: +1 204 474 7982; fax: +1 204 474 7623.
E-mail address: fayek@cc.umanitoba.ca (M. Fayek).

0012-821X/$ – see front matter © 2011 Elsevier B.V. All rights reserved.
doi:10.1016/j.epsl.2011.11.033

Table 1
Electron microprobe analysis of spherules and matrix of particles 1 and 2 from the >400 μm size magnetic fraction.

Spherules-particle 1																		Particle 2
	sph1	sph2	sph3	sph4	sph5	sph6	sph7	sph8	sph9	sph10	sph11	sph12	sph13	sph14	sph15	avg	std	sph1
Na_2O	0.13	0.27	0.34	0.38	0.23	0.18	0.05	0.14	0.25	0.26	0.51	0.15	0.20	0.12	0.14	0.22	0.12	0.19
MgO	0.35	0.24	0.23	0.29	0.28	0.26	0.28	0.25	0.31	0.35	0.32	0.40	0.25	0.32	0.28	0.30	0.05	0.41
Al_2O_3	0.53	0.98	0.85	0.76	0.69	0.58	0.52	0.57	0.97	1.31	1.45	0.72	0.72	0.63	0.57	0.79	0.28	0.86
SiO_2	6.47	8.50	7.18	7.34	6.81	7.01	6.34	6.96	6.98	8.69	10.35	7.83	6.20	6.53	6.57	7.32	1.12	10.19
SO_2	0.42	0.42	0.54	0.45	0.58	0.38	0.49	0.91	0.36	0.22	0.35	0.37	1.26	1.35	1.88	0.67	0.47	0.16
K_2O	0.01	0.08	0.03	0.04	0.04	0.02	0.02	0.01	0.02	0.04	0.07	0.01	0.03	0.01	0.02	0.03	0.02	0.03
CaO	1.67	1.96	1.69	1.63	1.60	1.82	1.73	1.80	1.98	1.99	2.03	2.19	1.61	1.61	1.55	1.79	0.20	3.08
TiO_2	0.02	0.05	0.00	0.02	0.02	0.02	0.01	0.04	0.03	0.03	0.03	0.02	0.02	0.01	0.03	0.02	0.01	0.11
Cr_2O_3	0.01	0.02	0.02	0.01	0.03	0.02	0.00	0.03	0.01	0.01	0.00	0.08	0.00	0.07	0.02	0.02	0.02	0.05
MnO	0.01	0.00	0.00	0.00	0.03	0.00	0.02	0.00	0.02	0.02	0.00	0.00	0.00	0.00	0.01	0.00	0.02	0.00
Fe_2O_3	81.63	67.10	78.69	75.84	82.56	80.18	75.22	79.28	76.69	73.97	71.51	79.59	80.43	82.16	82.35	77.81	4.44	71.24
NiO	0.00	0.00	0.01	0.01	0.00	0.00	0.00	0.03	0.00	0.02	0.00	0.00	0.00	0.00	0.00	0.00	0.02	0.02
V_2O_3	1.55	1.23	1.57	1.26	1.56	1.61	1.51	1.58	1.53	1.84	1.51	1.51	1.66	1.58	1.23	1.52	0.17	2.02
Total	92.80	80.85	91.14	88.01	94.43	92.08	86.18	91.60	89.15	88.76	88.14	92.88	92.37	94.38	94.63	90.49	3.73	88.36
Atom percent																		
Na	0.140	0.319	0.357	0.420	0.235	0.191	0.056	0.146	0.276	0.278	0.547	0.159	0.207	0.119	0.147	0.24	0.13	0.201
Mg	0.285	0.214	0.192	0.245	0.225	0.213	0.243	0.208	0.259	0.294	0.268	0.323	0.204	0.253	0.218	0.24	0.04	0.338
Al	0.340	0.701	0.552	0.507	0.435	0.373	0.355	0.370	0.640	0.861	0.944	0.459	0.460	0.397	0.358	0.52	0.19	0.559
Si	3.516	5.175	3.941	4.161	3.629	3.828	3.703	3.813	3.918	4.837	5.727	4.210	3.375	3.474	3.480	4.05	0.68	5.648
S	0.212	0.242	0.277	0.238	0.289	0.195	0.267	0.468	0.192	0.112	0.182	0.188	0.645	0.675	0.933	0.34	0.23	0.086
K	0.007	0.063	0.023	0.025	0.028	0.013	0.013	0.004	0.014	0.032	0.048	0.005	0.017	0.008	0.017	0.02	0.02	0.019
Ca	0.974	1.279	0.994	0.989	0.912	1.065	1.081	1.057	1.190	1.189	1.203	1.263	0.936	0.916	0.878	1.06	0.13	1.832
Ti	0.009	0.024	0.002	0.010	0.009	0.009	0.003	0.016	0.012	0.012	0.012	0.008	0.006	0.005	0.010	0.01	0.01	0.047
Cr	0.003	0.008	0.007	0.003	0.013	0.007	0.001	0.012	0.004	0.003	0.00	0.033	0.002	0.030	0.006	0.01	0.01	0.021
Mn	0.003	0.002	0.001	0.00	0.014	0.000	0.011	0.000	0.010	0.009	0.00	0.000	0.000	0.00	0.004	0.00	0.01	0.00
Fe	33.41	30.74	32.51	32.37	33.10	32.94	33.06	32.66	32.38	30.97	29.77	32.22	32.94	32.91	32.84	32.32	1.03	29.72
Ni	0.00	0.000	0.004	0.004	0.00	0.00	0.001	0.011	0.00	0.009	0.00	0.00	0.00	0.00	0.00	0.00	0.01	0.008
V	0.677	0.598	0.690	0.572	0.667	0.705	0.707	0.693	0.690	0.822	0.671	0.650	0.726	0.674	0.524	0.67	0.07	0.899

sph = spherules

Matrix-particle 1																		Particle 2 Spherule 2	
	1	2	3	4	5	6	7	8	9	10	11	12	13	14	15	avg	std	1	2
Na_2O	0.07	0.14	0.19	0.11	0.17	0.16	0.19	0.40	0.15	1.02	0.75	0.78	0.45	0.16	0.14	0.33	0.30	0.00	0.00
MgO	0.56	0.45	0.60	0.51	0.52	0.61	1.43	0.69	0.51	1.56	1.61	1.00	0.93	0.62	0.48	0.80	0.41	0.00	0.00
Al_2O_3	2.12	2.05	2.50	2.04	1.34	2.96	3.80	2.58	2.91	9.85	8.84	5.09	5.78	2.79	1.43	3.74	2.59	0.01	0.02
SiO_2	14.48	13.04	14.42	12.41	12.54	13.94	17.68	14.87	15.75	33.62	24.21	17.45	18.74	15.24	12.30	16.71	5.61	96.20	97.37
SO_2	0.12	0.07	0.10	0.06	0.11	0.07	0.10	0.14	0.06	0.41	0.62	0.78	0.33	0.08	0.22	0.22	0.22	0.01	0.00
K_2O	0.05	0.07	0.12	0.10	0.01	0.26	0.31	0.15	0.18	2.52	0.75	0.48	0.50	0.20	0.02	0.38	0.63	0.01	0.06
CaO	3.45	2.86	3.28	3.23	4.19	3.18	3.27	3.44	2.52	3.23	4.30	5.70	3.49	3.38	4.17	3.58	0.76	0.06	0.07
TiO_2	0.16	0.11	0.15	0.18	0.06	0.13	0.20	0.12	0.18	0.19	0.23	0.18	0.19	0.12	0.08	0.15	0.05	0.00	0.01
Cr_2O_3	0.10	0.00	0.02	0.00	0.09	0.00	0.04	0.00	0.01	0.00	0.04	0.00	0.03	0.00	0.06	0.01	0.05	0.00	0.00
MnO	0.00	0.02	0.02	0.02	0.00	0.00	0.02	0.00	0.00	0.00	0.00	0.00	0.01	0.03	0.00	0.00	0.02	0.03	0.03
Fe_2O_3	64.15	56.45	55.34	54.30	67.64	52.61	50.33	58.88	49.76	31.68	40.95	44.80	49.02	50.40	56.25	52.17	8.86	0.28	0.48
NiO	0.01	0.01	0.02	0.03	0.00	0.00	0.01	0.00	0.01	0.00	0.00	0.00	0.02	0.01	0.03	0.00	0.02	0.01	0.00
V_2O_3	2.49	3.07	2.61	3.14	2.62	2.64	2.19	3.28	2.25	1.34	1.87	2.44	2.47	2.41	2.22	2.47	0.49	0.00	0.01
Total	87.76	78.34	79.37	76.12	89.28	76.55	79.58	84.55	74.26	85.41	84.19	78.69	81.96	75.45	77.39	80.59	4.67	96.61	98.05

Table 1 (*continued*)

	Matrix-particle 1																Particle 2 Spherule 2	
	1	2	3	4	5	6	7	8	9	10	11	12	13	14	15	avg	std	1	2
Atom percent																			
Na	0.075	0.169	0.220	0.137	0.176	0.183	0.209	0.429	0.176	0.930	0.733	0.850	0.470	0.190	0.165	0.34	0.28	0.00	0.002
Mg	0.451	0.402	0.527	0.470	0.418	0.555	1.203	0.568	0.465	1.092	1.205	0.840	0.754	0.561	0.435	0.66	0.29	0.00	0.000
Al	1.346	1.455	1.729	1.492	0.851	2.116	2.534	1.682	2.112	5.451	5.225	3.379	3.695	2.005	1.036	2.41	1.42	0.003	0.008
Si	7.804	7.862	8.467	7.697	6.753	8.459	10.01	8.216	9.709	15.78	12.14	9.836	10.16	9.289	7.541	9.32	2.25	33.247	33.187
S	0.061	0.041	0.057	0.035	0.055	0.040	0.055	0.070	0.035	0.180	0.291	0.412	0.167	0.048	0.124	0.11	0.11	0.004	0.00
K	0.036	0.053	0.091	0.079	0.004	0.201	0.227	0.103	0.138	1.507	0.478	0.342	0.347	0.157	0.012	0.25	0.37	0.007	0.027
Ca	1.991	1.847	2.061	2.147	2.416	2.068	1.983	2.036	1.663	1.623	2.310	3.439	2.026	2.209	2.738	2.17	0.45	0.021	0.027
Ti	0.066	0.051	0.067	0.085	0.026	0.060	0.087	0.048	0.083	0.067	0.087	0.076	0.079	0.056	0.038	0.07	0.02	0.00	0.001
Cr	0.041	0.00	0.010	0.00	0.036	0.00	0.019	0.00	0.007	0.00	0.017	0.00	0.014	0.00	0.028	0.00	0.02	0.000	0.001
Mn	0.00	0.009	0.008	0.009	0.002	0.00	0.009	0.00	0.001	0.00	0.001	0.00	0.007	0.015	0.00	0.00	0.01	0.010	0.009
Fe	26.01	25.61	24.45	25.35	27.42	24.03	21.45	24.48	23.08	11.19	15.45	19.00	20.00	23.11	25.95	22.44	4.42	0.072	0.123
Ni	0.004	0.004	0.010	0.013	0.00	0.00	0.006	0.00	0.003	0.00	0.00	0.00	0.008	0.005	0.014	0.00	0.01	0.002	0.001
V	1.075	1.482	1.228	1.562	1.129	1.283	0.993	1.453	1.110	0.505	0.754	1.101	1.072	1.176	1.094	1.13	0.27	0.001	0.002

as the YD black mats, nor are they known to be associated with any major climatic perturbation as is the case with YD cooling.

At Murray Springs (MS), Arizona, a well-studied Clovis site contains a 2–10 cm thick black mat that covers the remains of two complete mammoths and twelve bison along with Clovis-age stone tools (Firestone et al., 2007; Haynes, 2008; Haynes and Huckell, 2007; West and Goodyear, 2008). The black mat covers a Clovis-age stream channel of sand and gravel as thin black stringers separated by several centimeters of white marl facies (Haynes et al., 2010). Away from the channel the black mat rises gently over an older surface where it is up to 10 cm thick (Haynes and Huckell, 2007). Recently, the mineralogy of the base of the black mat at this location has become of interest because of the reported occurrence of abundant magnetic spherules, peaks in iridium, and nanodiamonds considered to have formed during a cosmic impact event (Firestone et al., 2007; Kennett et al., 2008, 2009; West and Goodyear, 2008). Other researchers examined the samples from the same unit and suggested that none of these conclusions were warranted (Haynes et al., 2010; Paquay et al., 2009; Pinter and Ishman, 2008; Surovell et al., 2009). We, therefore, obtained magnetic fractions from this sediment to further characterize the materials.

2. Methods

In order to analyze the magnetic fraction of the black mat material, approximately 500 g of sample (26MS07) were obtained from the Murray Springs site. Sample 26MS07 included about 0.5 cm of basal black mat and about 1.0 cm of the top of stratum of the brown sandy clay unit directly below and in contact with the black mat (see Haynes et al., 2010 for a stratigraphy). These were dried and lightly disaggregated, and spread thinly on a large flat surface. A high field Nd magnet was then wrapped in plastic shrink-wrap and lightly touched to the surface of the powder under water. The material adhering to the wrapped magnet was then placed in a separate container. This magnetic fraction (729 mg) was then sieved into several size fractions. Portions of the finer fractions (~50 μm) were then examined using scanning electron microscopy. Coarser fractions (>400 μm) were mounted in epoxy mounts and polished for chemical and petrographic characterization.

2.1. Optical and Scanning Electron Microscope (SEM)

The initial, finer-grained samples were examined using a Hitachi S3400 variable pressure scanning electron microscope (SEM) in both backscattered and secondary electron modes. The epoxy mounts were first examined using a Nikon Eclipse 50i POL polarizing microscope, then coated with carbon to create a conductive surface and analyzed using a Cambridge Stereoscan 120 SEM. The electron microscope was equipped with a back-scattered electron detector as well as an energy dispersive X-ray spectrometer (EDS) with digital imaging capabilities. The SEM was used to characterize textures, sample surfaces and obtain backscatter electron images of the samples to determine the mineralogy of the particles.

2.2. Electron Microprobe (EMP)

Electron microprobe analyses were obtained using a Cameca SX100 electron microprobe (EMP) with a Princeton Gamma Tech (PGT) equipped with an energy dispersive spectrometer and five wavelength dispersive spectrometers. A 5-μm beam operated at an acceleration of 15 keV with a 20 nA current was used. Thirteen elements were analyzed and quantitative analyses of the matrix and spherules are reported in Table 1.

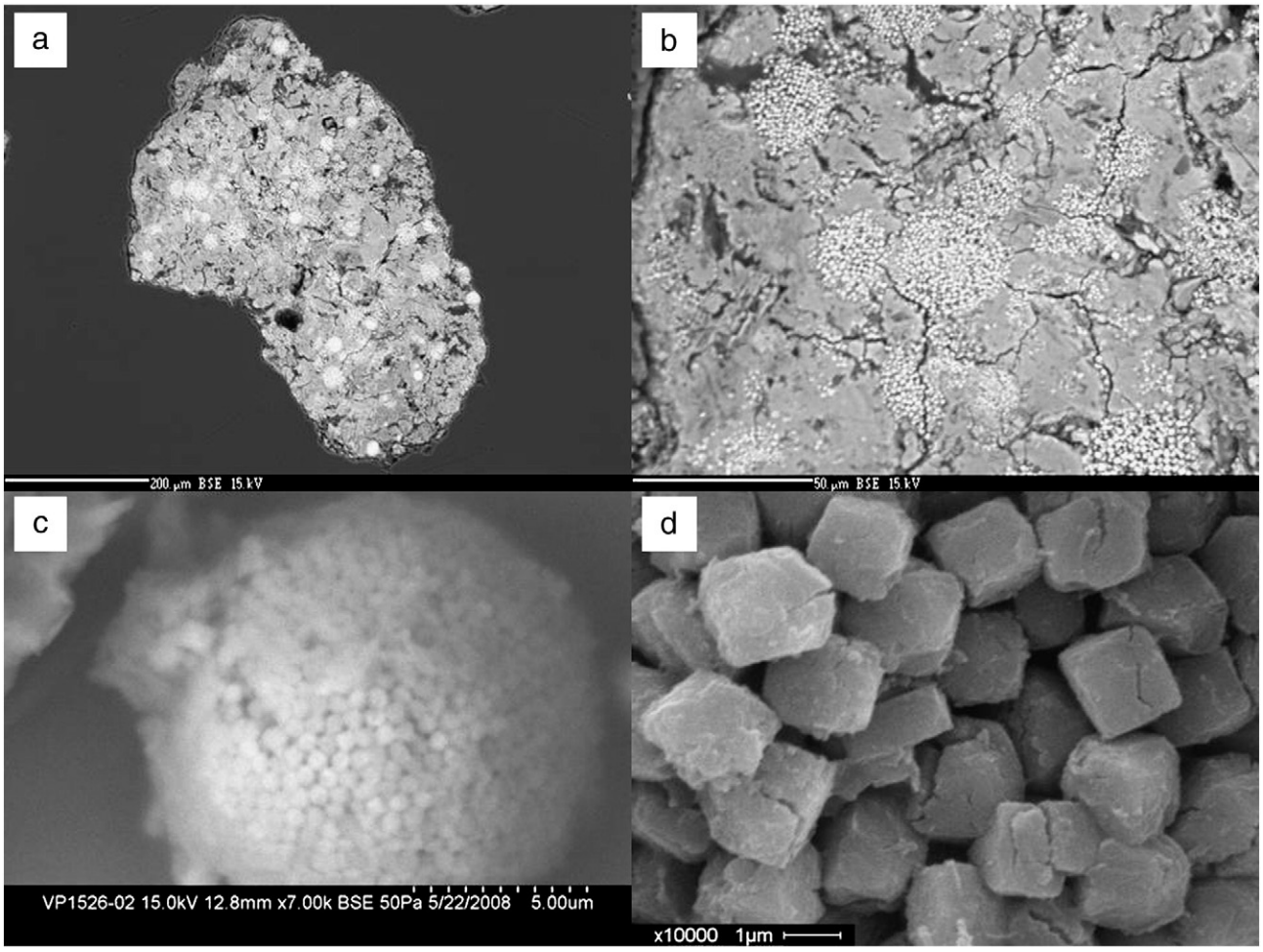

Fig. 1. Petrography of particles and iron spherules from the Murray Springs, AZ Clovis-age site. (a) A back-scattered electron (BSE) image of a particle from the >400 µm magnetic fraction obtained from the basal portion of the black mat at the Murray Springs Clovis-age site showing iron spherules (bright gray) in an iron–silicon glass matrix (darker gray), (b) a magnified BSE image showing the texture of the spherules enclosed in glassy matrix, (c) a SEM image of whole iron spherule from the 180 µm size fraction, and (d) a scanning electron image (SEM) of the grains (often cracked) that constitute the iron spherules.

2.3. High-Resolution Transmission Electron Microscopy (HRTEM)

Following SEM imaging, high-resolution transmission electron microscopy (HRTEM) and EDS analyses were employed to better characterize both the glass and framboidal particles. To do so, samples were prepared using an Hitachi FB-5000 dual-beam focussed-ion-beam (FIB) microsampling mill to obtain electron-transparent samples of iron oxide subgrains from the framboids and from the glassy matrix (described below). These were imaged using the Hitachi HF-3300 with a double-tilt sample holder at the High-Temperature Materials Laboratory at the Oak Ridge National Laboratory (HTML).

3. Results

Fig. 1 shows SEM images of some of the framboids discovered in these samples (spherules are referred to as framboids or having a framboidal texture when they appear as a cluster of smaller oxide particles). These particles are significantly different from the smooth spheroids previously described by Firestone et al., 2007, which were reported to form a distinct abundance peak in this layer at Murray Springs (Firestone et al., 2007; Haynes et al., 2010). While the framboids, approximately 5 and 50 µm in diameter, appear to be spherical and smooth, closer SEM examination (Fig. 1c, d) revealed that the surfaces are not smooth, but are rough because they are made up of small (~1 µm) cubic subgrains. These subgrains have morphologies consistent with magnetite, consisting of a cube modified in some

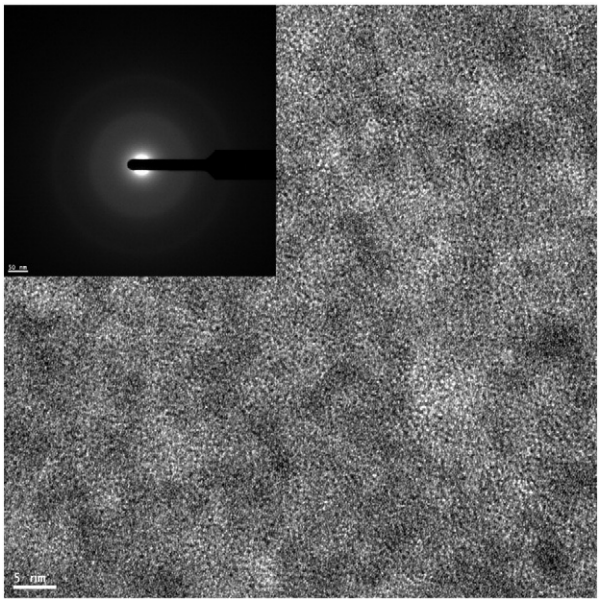

Fig. 2. A high-resolution transmission electron microscope image (HRTEM) of glassy matrix showing randomly oriented, nanoparticulate crystalline material with an electron diffraction pattern showing rings (inset) characteristic of a non-crystalline matrix.

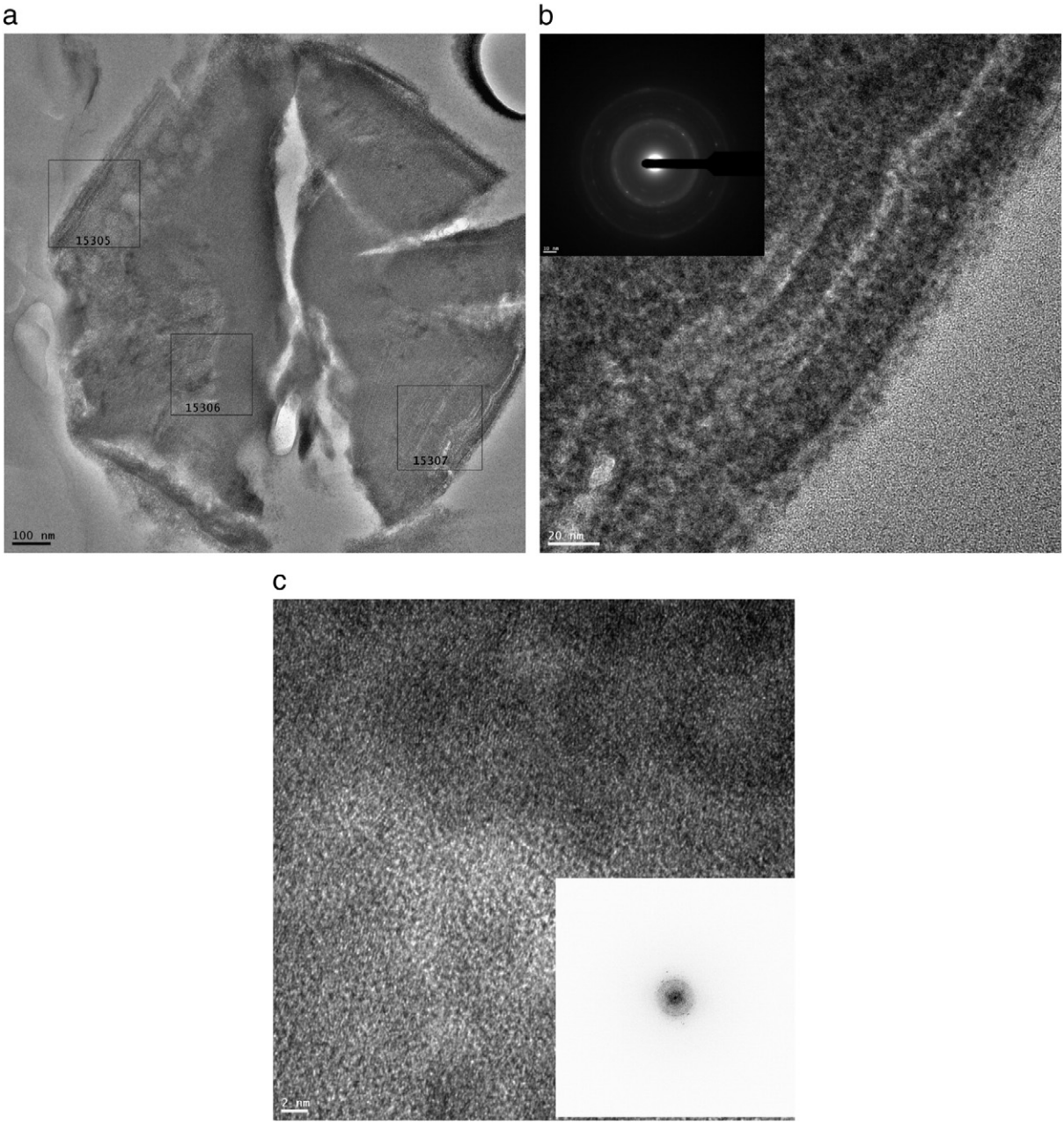

Fig. 3. (a) A transmission electron image of a framboid grain showing structurally complex zones, containing significant internal layering and strong fracture patterns consistent with the SEM results (see Fig. 1). Squares show locations of high-resolution TEM images obtained; (b) HRTEM image of square 15307 in (a) showing the structural complexity of the framboid and the electron diffraction pattern (inset); (c) HRTEM image of the framboid showing randomly oriented, nanoparticulate crystalline material similar to that of the glassy matrix, and Fourier transform analysis of this image (inset) with three periodicities and d-spacings consistent with hematite.

cases by octahedral and/or dodecahedral faces. Energy dispersive spectroscopy analysis revealed that they are, indeed, iron oxides. In addition, most of the grains appeared to be cracked (Fig. 1d). Such magnetite framboids are quite unusual in terrestrial environments, but are similar to those found in several types of chondritic meteorites, including CI, CR, and CM chondrites as well as CS-type cosmic dust (see discussion below).

When we examined the larger (>400 μm) size fraction we also found large particles containing framboidal iron oxide spherules. In this case, however, the particles were contained within a glassy matrix (Fig. 1a, b). The results of HRTEM analysis of both the matrix and framboid particles are shown in Figs. 2 and 3. Electron diffraction analysis of the glass yielded only faint ring structures at small d-spacings. This is consistent with high resolution imaging and showed that the glass is composed of randomly oriented crystalline nanoparticles approximately 2 nm across in an otherwise amorphous matrix.

TEM analysis was also performed on the framboidal particles. Fig. 3a shows that these particles are structurally complex, containing significant internal layering and strong fracture patterns similar to those observed in the SEM. Electron diffraction (Fig. 3b inset), however, indicates that these particles are iron-rich spinels that are largely amorphous in character. Only a few, faint diffraction spots and low d-spacing diffuse ring structures are present. As with the glass, high-resolution imaging (Fig. 3c) again shows the presence of orientationally-disordered nanoparticles. Fourier transform analysis of this image yields only three periodicities, but the d-spacings of these points are similar to hematite.

The compositions of both the framboids and the matrix were determined by electron microprobe analysis (Table 1). The framboids are iron-rich, vanadium and calcium-bearing, and largely devoid of titanium. This is significantly different from that of the spherules previously documented by Firestone et al., 2007, from the base of the black mats, but similar to compositions of spinels from chrondrites.

Comparisons of these results with analyses of carbonaceous chondrites, impact material associated with meteorite showers and meteorite craters, and tektites are shown in Fig. 4a and b (see SI Table 1). The glass matrix is Fe-oxide rich, and has a Si content consistent with that of material from meteorite showers (Brett, 1967; Miura et al., 1999; Miura et al., 2000) (Fig. 4a, b). The Fe/Si ratio is far too high to be consistent with any known mineral, (Fig. 4c), but is similar to the composition of the eutectic point in the SiO_2–Fe_3O_4 system with a melting point of approximately 1500 °C (Bowen and Schairer, 1932). Such a high formation temperature is only consistent with impact or fulguritic conditions, but the chemistry of the glasses (see SI Table 1) is vastly different from that of terrestrial fulgurites (Essene and Fisher, 1986) (Fig. 4c).

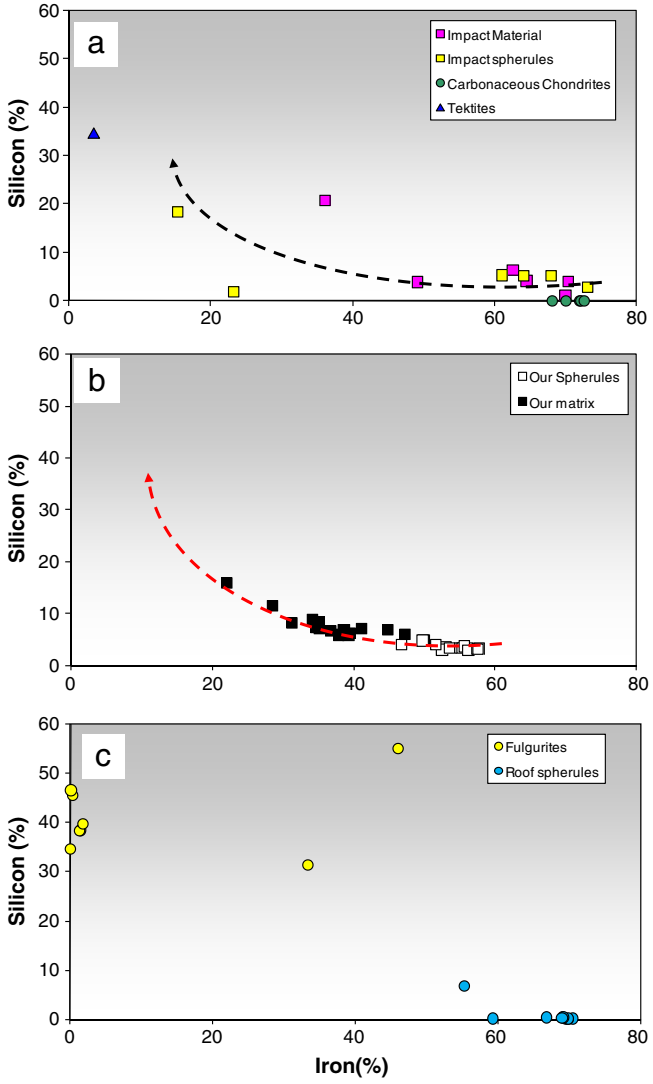

Fig. 4. Iron vs. silicon diagrams (Data from Table 1). (a) Extra-terrestrial material including spherules found in carbonaceous chondrites, impact material from meteorite showers and craters, and tektites (fused particles of the Earth's surface formed during a meteorite impact), (b) our data from the Murray Springs material showing both the matrix compositions as well as the iron spherules, and (c) spherules found in terrestrial environments such as fulgurites, and Professor Haynes' roof.

Table 2
Concentrations of selected elements from extra terrestrial and terrestrial material.

Sample description	Si	Ca	Ti	Fe	Source
Carbonaceous chondrite	0	0.11	0.11	72.1	Miura et al., 2000
	0	0.04	0	72.3	
	0	0.3	0	72.8	
	0.01	0	0	70.1	
	0.05	0.07	0	68.2	
Impact material	6.35	0.85	0	62.71	Zhao et al., 2006
	20.77	0.92	0	36.27	
	1.18	0	0	70.12	
	4.09	0	0	64.66	
	3.85	0	0	49.3	
	4.04	0	0	70.51	
Impact spherules	5.17	0	0	64.27	Pósfai et al., 2001
	5.26	0	0	68.09	
	1.97	0	0	23.4	
	18.47	0	0	15.52	
	2.82	0	0	73.24	
	5.36	0	0	61.15	
Average tektite	34.78	1.56	0.45	3.61	Beckerling and Bischoff, 1995
Fulgurites	38.45	1.28	0.12	1.48	Pinter and Ishman, 2008
	38.25	0.64	0.24	1.4	
	39.69	0.99	0.3	1.79	
	45.45	0.14	0.66	0.39	
	46.48	0	0	0.16	
	99.7	0	0	0.2	
	54.9	0	0	45.9	
	34.6	0	0	0.1	
	31.4	0	29.8	33.3	
Roof spherules	0.06	0.02	0.04	69.50	Haynes et al., 2010
	0.12	0.00	0.05	70.44	
	6.68	0.32	0.24	55.25	
	0.33	0.02	0.27	66.75	
	0.09	0.02	4.58	59.26	
	0.09	0.01	0.09	69.85	
	0.15	0.03	0.04	69.81	
	0.33	0.00	0.13	69.00	
	0.40	0.01	0.17	69.19	
	0.23	0.01	0.11	68.93	

4. Discussion

The data obtained on the framboids from MS strongly suggest that they are not only of meteoritic origin, but that they are relicts of a hypervelocity impact. As noted above, it has been suggested that some of the particles that were reportedly recovered from YD black mats may have originated as accumulations of cosmic dust. To test this possible origin for the particles recovered in this study, we examined the magnetic fraction of samples collected from the roof top of the home of Professor Haynes in Tucson, Arizona, approximately ~80 miles northwest of the MS site (Haynes et al., 2010). Although iron-oxide spherules were found in the roof-top samples, these particles did not have the framboidal texture observed in the MS samples and their chemistry (Table 2) (Haynes et al., 2010) was significantly different from that of the particles from MS (Table 2; Fig. 4c). In addition, none of the particles obtained were embedded in glassy matrices.

The presence of the glassy matrix is especially significant. Cosmic dust (Brownlee, 1985) continually falls on the Earth's surface. It is made up of ET particles such as interplanetary dust particles (IDPs) (Dai and Bradley, 2001) and micrometeorites (Badjukov and Raitala, 2003; Beckerling and Bischoff, 1995; Kurat et al., 1994). These particles can consist of smooth iron, silica, and glass and framboidal micro-spherules and particles in a crystalline matrix (Badjukov and Raitala, 2003; Beckerling and Bischoff, 1995; Brownlee, 1985; Dai and Bradley, 2001; Kurat et al., 1994). Framboidal magnetite has, in fact, been reported from CS-type (chondritic, smooth) cosmic dust. To our knowledge, however, framboidal magnetites such as those

reported here have never been reported in a glassy matrix in cosmic dust.

CS-type cosmic dust is believed to have originated as chondritic meteorites (Hua and Buseck, 1998). While rare, framboidal spherules consisting of magnetite crystals are found in a variety of chondritic extraterrestrial materials. These include the CI-type chondrites, of which only nine are currently known including Orgueil (Abreu and Brearly, 2005; Hua and Buseck, 1998), which are believed to have undergone aqueous alteration, the CR chondrites of which only about 15 are known (Hyman et al., 1985), the CM chondrites Essebi and Haripura (Hyman et al., 1985), and other chondrites in which the magnetite framboids have sulfide rims (Boctor et al., 2003; Rubin and Kallemeyn, 1990). Again, to the best of our knowledge these framboids do not occur in glassy matrices in any of these meteorite types.

Magnetite framboids are also found in some terrestrial materials but, again, these are quite rare. In terrestrial materials, such as iron ore formations (Lougheed and Mancuso, 1973) and dinosaur bones (Miura et al., 1999) the Fe-rich framboids are usually pseudomorphically replacing biogenic sulfides and therefore have high sulfur contents (e.g., Pósfai et al., 2001). Micro-spherules are also found in fulgurites, which are fused Earth material formed when lightning strikes the Earth, but these micro-spherules rarely have a framboidal texture, have an extensive range in chemistry (Fig. 2c) including high Ti values, and are often highly reduced (Essene and Fisher, 1986). Iron-oxide framboids have also been described among the many textures and compositions of “ferrospheres” in fly ashes, possibly as pseudomorphs after pyrite (Zhao et al., 2006), but these appear to compare poorly to those in our samples and, again, may contain significant sulfur. Thus, the particles described in this study are not consistent with samples from either terrestrial or unmodified extraterrestrial sources. Therefore, as the framboidal magnetites in a glassy matrix reported here are consistent with those found in some chondritic meteorites, and inconsistent with known terrestrial sources, it is possible that they could have formed as the result of the high-energy destruction of an appropriate chondritic meteorite. Together, these data suggest that the framboid particles are the product of a hypervelocity impact event. Its spatial extent remains to be determined (c.f. Bunch et al., 2011).

5. Conclusions

Analysis of the data presented in this paper clearly shows that the framboidal particles obtained from the MS site are not consistent with known cosmic dust or terrestrial materials. These particles occur in a glassy matrix with an unusual chemical composition, are structurally complex, and contain significant internal layering and strong fracture patterns. Such fracturing could reflect shock damage that occurred during an impact event. While the fracturing of the oxide particles, and possibly their amorphization could be due to alteration and expansion during partial or complete alteration to an iron hydroxide or oxy-hydroxide in the moist soil environment typical of the black mat, this is an unlikely origin for the glassy matrices in which the oxide particles occur. In addition, when glasses are subject to alteration they tend to devitrify and crystallize. Neither texture is observed in the glassy matrix of the particles in our study. These data suggest that the observed textures are not due to hydrational expansion, but to a shock event that fractured and largely amorphised the grains as a whole and melted and possibly contaminated the matrix. Therefore, we argue that these particles are the product of a hypervelocity impact event. The exact nature of this event, and its spatial extent, however, remain to be determined.

Acknowledgments

Support for this research was provided by a NSERC-discovery, CRC, and CFI grants to Fayek. Research was also sponsored by the Division of Chemical Sciences, Geosciences and Biosciences, Office of Basic Energy Sciences, U.S. Department of Energy. We thank Laura Bergen, Brandi Shabaga, Panseok Yang and Sergio Mejia at UM, and Larry Walker and Emily Simonds at ORNL for their help in obtaining the images and chemical analyses. We would also like to thank Dr. C. Vance Haynes, who collected the material we looked at in this study, and initiated our interest in this work.

References

Abreu, N.M., Brearly, A.J., 2005. Mineralogical characterization of the matrices of the primitive CR chondrites MET00426 and EET99177. Meteorol. Planet. Sci. 40, 5332.
Alley, R.B., 2000. The Younger Dryas cold interval as viewed from central Greenland. Quat. Sci. Rev. 19, 213–226.
Alley, R.B., 2007. Wally was right: Predictive ability of the North Atlantic “conveyor belt” hypothesis for abrupt climate change. Annu. Rev. Earth Planet. Sci. 35, 241–272.
Badjukov, D.D., Raitala, J., 2003. Micrometeorites from the northern ice cap of the Novaya Zemlya archipelago, Russia: the first occurrence. Meteorol. Planet. Sci. 38, 329–340.
Beckerling, W., Bischoff, A., 1995. Occurrence and composition of relict minerals in micrometeorites from Greenland and Antarctica-implications for their origins. Planet Space Sci. 43, 435–449.
Boctor, N.Z., Kurat, G., D'Alexander, C.M.O., 2003. Sulfide-oxide assemblage in Tagish Lake carbonaceous chondrite. Lunar Planet. Sci. 34, 1705.
Bowen, N.L., Schairer, J.F., 1932. The system FeO–SiO2. Am. J. Sci. 24, 177–213.
Bradley, R.S., England, J.H., 2008. The Younger Dryas and the sea of Ancient ice. Quat. Res. 70, 1–10.
Brett, R., 1967. Metallic spherules in impactite and tektite glasses. Am. Mineralog. 52, 721–733.
Broecker, W.S., 2006. Was the Younger Dryas triggered by a flood? Nature 312, 1146–1148.
Broecker, W.S., Peteet, D.M., Rind, D., 1985. Does the ocean–atmosphere system have more than one stable mode of operation. Nature 315, 21–26.
Broecker, W.S., Kennett, J.P., Trumbore, S., Bonani, G., Woelfli, W., 1989. Routing of meltwater from the Laurentide ice sheet during the Younger Dryas cold episode. Nature 341, 318–321.
Brownlee, D.E., 1985. Cosmic dust: collection and research. Annu. Rev. Earth Planet. Sci. 13, 147–173.
Bunch, T.E., Wittke, J., West, A., Kennett, J., 2011. Shock-melt evidence for a cosmic impact with Earth during the Younger Dryas at 12.9 ka. Abstract 1606, Session 60, XVIII INQUA-Congress, 21–27 July, Bern, Switzerland.
Dai, Z.R., Bradley, J.P., 2001. Iron–nickel sulphides in anhydrous interplanetary dust particles. Geochim. Cosmochim. Acta 65, 3601–3612.
Essene, E., Fisher, D.C., 1986. Lightning strike fusion: extreme reduction and metal-silicate liquid immiscibility. Science 234, 189–193.
Fiedel, S.J., 2006. Points in time: establishing a precise hemispheric chronology for Paleoindian migrations. In: Morrow, J.E., Gnecco, C. (Eds.), Paleoindian Archaeology. Univ. of Florida Press, Gainesville, FL, pp. 21–43.
Firestone, R.B., West, A., Kennett, J.P., Becker, L., Bunch, T.E., Revay, Z., Schultz, P.H., Belgya, T., Dickenson, O.J., Erlandson, J.M., Goodyear, A.C., Harria, R.S., Howard, G.A., Kennett, D.J., Kloosterman, J.B., Lechler, P., Montgomery, J., Poreda, R., Darrah, T.H., Que Hee, S.S., Smith, A.R., Stich, A., Topping, W., Wittke, J.H., Wolback, W.S., 2007. Evidence for an extraterrestrial impact 12,900 years ago that contributed to the megafaunal extinctions and the Younger Dryas cooling. Proc. Natl. Acad. Sci. 104, 16016–16021.
Gill, J.L., Williams, J.W., Jackson, S.T., Lininger, K.B., Robinson, G.S., 2009. Pleistocene megafaunal collapse, novel plant communities, and enhanced fire regimes in North America. Science 326, 1100–1103.
Haynes Jr., C.V., 2008. Younger Dryas “black mats” and the Rancholabrean termination in North America. Proc. Natl. Acad. Sci. 105, 6520–6525.
Haynes Jr., C.V., Huckell, B.B., 2007. Murray Springs, a Clovis site with multiple activity in areas in the San Pedro Valley, Arizona. Anthropological Papers of the University of Arizona no.7. University of Arizona Press, Tucson, AZ.
Haynes Jr., C.V., Boerner, J., Domanik, K., Lauretta, D., Ballenger, J., Goreva, J., 2010. The Murray Springs Clovis site, Pleistocene extinction, and the question of extraterrestrial impact. Proc. Natl. Acad. Sci. U. S. A. 107, 4010–4015.
Holliday, V.T., Meltzer, D.J., 2010. The 12.9ka impact hypothesis and North American Paleoindians. Curr. Anthropol. 51, 575–585.
Hua, X., Buseck, P.R., 1998. Unusual forms of magnetite in the Orgueil carbonaceous chondrite. Meteorol. Planet. Sci. 33, A215–A220.
Hyman, M., Ledger, E.B., Rowe, M.W., 1985. Magnetite morphologies in the Essebi and Haripura CM chondrites. J. Geophys. Res. 90, C710–C714.
Kennett, D.J., Kennett, J.P., West, G.J., Erlandson, J.M., Johnson, J.R., Hendy, I.L., West, A., Culleton, B.J., Jones, T.L., Stafford Jr., T.W., 2008. Wildfire and abrupt ecosystem disruption on California's northern Channel Islands at the Allerød-Younger Dryas boundary (130–12.9 ka). Quat. Sci. Rev. 27, 2530–2545.
Kennett, D.J., Kennett, J.P., West, A., Mercer, C., Que Hee, S.S., Bement, L., Bunch, T.E., Sellers, M., Wolback, W.S., 2009. Nanodiamonds in the Younger Dryas boundary sediment layer. Science 323, 94.
Kurat, G., Koeberl, C., Presper, T., Brandstatter, F., Maurette, M., 1994. Petrology and geochemistry of Antarctic micrometeorites. Geochim. Cosmochim. Acta 58, 3879–3904.
Lougheed, M.S., Mancuso, J.J., 1973. Hematite framboids in the Negaunee iron formation, Michigan: evidence for their biogenic origin. Econ. Geol. 68, 202–209.

Marlon, J.R., Bartlein, P.J., Walsh, M.K., Harrison, S.P., Brown, K.J., Edwards, M.E., Higuera, P.E., Power, M.J., Anderson, R.S., Briles, C., Brunelle, A., Carcaillet, C., Daniels, M., Hu, F.S., Lavoie, M., Long, C., Minckley, T., Richard, P.J.H., Scott, A.C., Shafer, D.S., Tinner, W., Umbanhowar Jr., C.E., Whitlock, C., 2009. Wildfire responses to abrupt climate change in North America. Proc. Natl. Acad. Sci. 106, 2519–2524.

McManus, J.F., Francois, R., Gherardi, J.M., Keigwin, L.D., Brown-Leger, S., 2004. Collapse and rapid resumption of Atlantic meridional circulation linked to deglacial climate changes. Nature 428, 834–837.

Meltzer, D.J., Holliday, V.T., 2010. Would North American Paleoindians have noticed Younger Dryas age climate changes? J. World Prehist. 23, 1–41.

Miura, Y., Fukuyama, S., Gucsik, A., 1999. Impact metamorphosed compositions of the Fe–Si–Ni–S system. Journal of Materials Processing Technology 85, 188–191.

Miura, Y., Fukuyama, S., Kedves, M.A., Yamori, A., Okamoto, M., Gucsik, A., 2000. Chemical separation of Fe–Ni particles after impact. Adv. Space Res. 25, 285–288.

Paquay, F.S., Goderis, S., Ravizza, G., Vanhaeck, F., Boyd, M., Surovell, T.A., Holliday, V.T., Hayned Jr., C.V., Claeys, P., 2009. Absence of geochemical evidence for an impact eveny at the Bølling-Allerød?Younger Dryas transition. Proc. Natl. Acad. Sci. U. S. A. 106, 21505–21510.

Pinter, N., Ishman, S.E., 2008. Impacts, mega-tsunami, and other extraordinary claims. GSA Today 18, 37–38.

Pósfai, M., Cziner, K., Márton, E., Márton, P., Buseck, P.R., Frankel, R., Bazylinski, D., 2001. Crystal-size distributions and possible biogenic origin of Fe sulfides. Eur. J. Mineralog. 13, 691–703.

Rubin, A., Kallemeyn, G.W., 1990. Lewis Cliff 85332: a unique carbonaceous chondrite. Meteoritics 25, 215–225.

Stuiver, M., Groots, P.M., Braziunas, T.F., 1995. The GISP2 $\delta^{18}O$ climate record of the past 16,500 years and the role of the sun, oceans and volcanoes. Quat. Res. 44, 341–354.

Surovell, T.A., Holliday, V.T., Gingerich, J.A.M., Ketron, C., Haynes Jr., C.V., Hilman, I., Wagner, D.P., Johnson, E., Claeys, P., 2009. Proc. Natl. Acad. Sci. U. S. A. 106, 18155–18158.

Taylor, K.C., Lamorey, G.W., 1993. The 'flickering switch' of late Pleistocene climate change. Nature 361, 432–435.

West, A., Goodyear, A.C., 2008. The Clovis comet. Mammoth Trumpet 23, 4.

Zhao, Y., Zhang, J., Sun, J., Bai, X., Zheng, C., 2006. Mineralogy, chemical composition, and microstructures of ferrospheres in fly ashes from coal combustion. Energy Fuel 20, 149–1497.